Hindawi
International Journal of Antennas and Propagation
Volume 2022, Article ID 8517646, 9 pages
https://doi.org/10.1155/2022/8517646

Research Article

A Low-Profile Broadband Circularly Polarized Metasurface Antenna Aperture Coupled by Shorted Annular-Ring Slot

Shuangbing Liu,[1,2] **Lixia Yang**,[2] **Qian Chen**,[2] **and Xianliang Wu**[2]

[1]*School of Electronic Engineering, Chaohu University, Hefei, China*
[2]*Information Materials and Intelligent Sensing Laboratory of Anhui Province, Anhui University, Hefei, China*

Correspondence should be addressed to Lixia Yang; lixiayang@yeah.net

Received 25 May 2022; Revised 13 July 2022; Accepted 15 July 2022; Published 10 August 2022

Academic Editor: Miguel Ferrando Bataller

A low-profile (LP) metasurface antenna is proposed for broadband circularly polarized (CP) operations. The metasurface radiator, formed by a 5×5 array of square patches, has a microstrip line fed at its bottom through a shorted annular-ring slot centered on the ground plane. First, the characteristic mode analysis (CMA) methodology is employed to examine the intrinsic modes of the metasurface. Subsequently, a pair of mutually orthogonal modes is selected and excited by the feeding structure with a 90° phase difference to produce CP radiation. For the purpose of verification, a prototype antenna is developed, and the obtained data reveal that the antenna exhibits an impedance bandwidth of 43.9% ranging from 4.8 to 7.5 GHz (S11<−10 dB). The 3-dB axial ratio bandwidth is 22.2% in the range of 5.6–7 GHz, among which a satisfactory left-handed CP radiation is achieved, and the maximum gain in the broadside direction reaches 9.3 dBic at 6.9 GHz.

1. Introduction

The circularly polarized (CP) antenna is broadly exploited in numerous communication systems due to the advantages of reducing the multipath effects as well as reducing polarization alignment between the receiver and the transmitter. The CP slot antennas are of considerable application in the present and future wideband wireless systems owing to their low profile (LP), low cost, easy integration, and wide impedance bandwidth. Various shaped slot antennas with wide 3-dB axial ratio (AR) bandwidth have been proposed in the literature, such as combined dual-square-ring-shaped slot antennas [1], and slot antennas loaded by multiple-circular-sector patches [2]. The CP radiation can also be attained by introducing a shorted section to a proper position along with the ring slot. The 3-dB AR bandwidths of about 8.4 and 8.1% have been obtained in order for annular and square slot antennas [3]. The antenna gains within the CP bandwidth for both types are about 4.0–5.6 dBic. In [4], two concentric shorted annular-ring slots are exploited to design dual-band CP antennas such that the 3-dB AR bandwidth for the upper (lower) band is 3% (1.5%). In addition, the shorted ring slots were exploited to excite the dielectric resonator antenna (DRA) with circular polarization [5, 6]. However, their main drawback was narrow AR bandwidth.

Recently, the metasurface has been employed in several novel antennas for AR bandwidth expansion and gain enhancement. In some antenna configurations, the metasurface is utilized as a reflector or a surface wave converter placed beneath the radiator [7–9], achieving broad CP bandwidth while complicating antenna structure. On the other hand, the metasurface is stacked directly on the radiator, thus retaining LP properties and providing wide AR bandwidths [10–13]. According to the research work in [10], a circularly polarized corner truncated square patch antenna using a metasurface exhibited an AR bandwidth of 23.4% and an LP of $0.056\lambda_0$. An H-shaped patch array (4×4) metasurface demonstrates a CP bandwidth of 14.3% and a profile of $0.071\lambda_0$ [11]. In order to enhance the radiation gain, an air layer [14] or a foam substrate [15] was placed between the metasurface and the feed structure. Nevertheless, this strategy leads to an increase in the profile height and the structural complexity of the antenna.

In the present paper, a CP metasurface antenna with LP is presented. A metasurface containing 5×5 square metal patches is implemented to improve the bandwidth and radiation gain. The modal current and the radiation properties of the designed metasurface are observed based on the CMA [16–18]. Two orthogonal modes are chosen as working modes to generate circularly polarized radiation. A single-feed structure composed of a microstrip line and a shorted annular-ring slot is applied to excite both orthogonal modes with a relative phase difference (PD) of 90°. The simulated and measured data are employed to validate the broadband CP and high-gain radiation effects of the developed antenna.

2. Configuration of the Antenna

The geometrical and structural dimensions of the developed antenna in order are presented in Figure 1 and Table 1. The antenna contains two different dielectric substrates. As demonstrated in Figure 1(a), a metasurface composed of a 5×5 array of square patches is deposed on the upper substrate with a dielectric constant of 3.5 and thickness $h_2 = 2$ mm. The feeding microstrip line is labeled on the bottom surface of the upper substrate with a dielectric constant of 4.4 and thickness $h_1 = 0.8$ mm. The ground metal plane with a shorted annular-ring slot is sandwiched between the two substrates (see Figure 1(b)). The ground plane is in direct contact with the two substrates to realize the LP characteristics, as demonstrated in Figure 1(d). So far as a single-feed annular slot antenna is concerned, the shorted section can be deemed as a perturbation segment, and the antenna can produce satisfactory CP radiation while the parameters (α_1, α_2) of the shorted section are properly determined.

3. Operating Mechanisms

3.1. Characteristic Mode Analysis of the Metasurface. In order to realize the operating mechanisms of the developed metasurface antenna, the intrinsic characteristic modes generated from the metasurface are explored by applying the CMA. The substrates and ground plane are assumed to be infinite. The PEC boundaries are set along the z-direction, and the open boundaries in other five directions have been shown in Figure 2. The metasurface patches are meshed to solve the electrical currents.

The characteristic mode analysis of the metasurface is carried out from 4 to 8 GHz firstly. The first four characteristic modes are chosen to analyze the modes of the antenna, while the higher order modes can hardly be excited at these frequencies as their modal significance is quite low. Figure 3 displays the modal significance and the characteristic angle of the four characteristic modes. The characteristic mode theory is described in detail in [19]. It can be concluded that the nearer the modal significance is to the maximum value of one or the characteristic angle is to 180°, the more effectively the associated mode contributes to radiation. Notably, J_1 and J_1' are a pair of modes resonating at 7.1 GHz with the same modal significance. The remaining two modes (i.e., J_2 and J_3) demonstrate similar resonant frequencies and share the same trends of variations against frequencies.

Figures 4(a)–4(d) present the corresponding modal electric currents at 6.8 GHz, where the black arrow shows the current direction. As can be seen from Figures 4(a) and 4(b), J_1 and J_1' are in phase throughout the whole metasurface and polarize in the x- and y-directions, respectively. Because of the metasurface symmetry, J_1 and J_1' represent a pair of orthogonal modes, and both of them radiate in the $+z$-direction (see Figures 5(a) and 5(b)). The currents J_2 and J_3 are self-symmetric along the x-axis and y-axis, respectively. This will lead to a radiation null at boresight (see Figures 5(c) and 5(d)). Consequently, J_1 and J_1' indicate the desired modes for the broadside radiation. A circular polarization is also detectable by exciting both orthogonal modes with a PD of 90° simultaneously.

3.2. Feeding Network Design. To retrieve circularly polarization radiation, J_1 and J_1' with a PD of 90° were simultaneously excited via an adaptive feed network. Figure 3 displays that the currents J_1 and J_1' are evenly distributed on the whole patches of the metasurface for the central patch, and the current density is mostly distributed at the edge of the patch. For J_2 and J_3, the current distribution is completely different, and the current distribution on the central unit is very weak. In view of these current distribution characteristics, the feed structure is placed at the metasurface's center patch. Therefore, J_1 and J_1' can be effectively excited, whereas J_2 and J_3 are suppressed. To satisfy these conditions, a single-feed network combined with a shorted annular-ring slot and a microstrip line for exciting the antenna are employed (Figures 1(b) and 1(c)).

In order to illustrate the operating mechanisms of CP radiation, the surface current distribution of the metasurface is examined. The currents are estimated for two AR points (5.8 and 6.8 GHz) of the 5×5 cell configuration and given in Figure 6. As demonstrated in Figure 6(a), the currents flow in the x- and y-directions in order at the phases of 0° and 90°. As illustrated in Figure 6(b), at the phases of 0° and 90°, the dominant current discharges in the x- and y-directions, respectively. It is demonstrated that both orthogonal modes with a PD of 90° are excited to realize the left-handed (LH) CP radiation for each AR point. In addition, the maximum currents occur on the metal plates located in the metasurface center at 5.8 GHz, while the maximum current occurs on all the constituent metasurface plates at 6.8 GHz. It implies that the current on the metasurface is stronger at 6.8 GHz than at 5.8 GHz. These results imply that the AR point at 6.8 GHz is chiefly attributed to the metasurface, while that at 5.8 GHz is produced by the shorted annular-ring slot.

3.3. Effect of Spacing between Elements of the Metasurface. A parametric study was carried out on variation of edge-to-edge spacing of metasurface elements. Figure 7(a) shows the S-parameters versus frequency for different spacing g. It is clear that there are two resonant frequencies within the impedance bandwidth for each spacing g. The operating frequency shift towards higher frequency as the spacing is increased. Figure 7(b) shows the AR versus frequency for different spacing g. It is observed that there are two AR

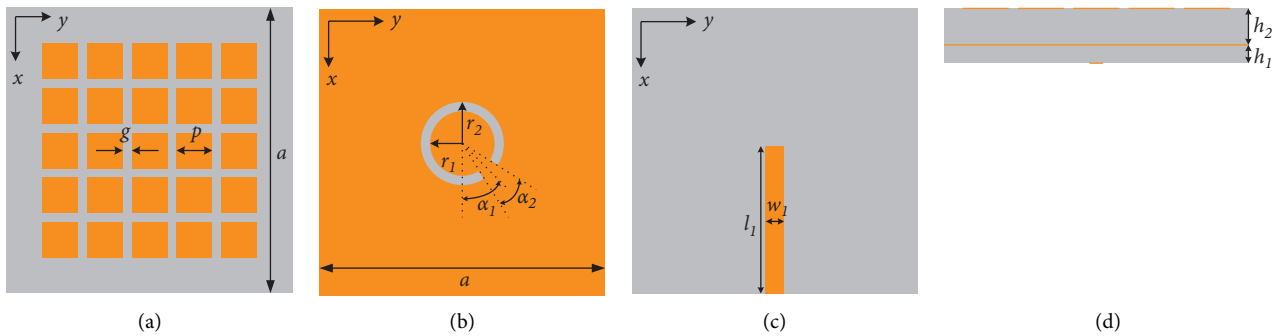

Figure 1: The configuration of antenna structure: (a) metasurface, (b) ground metal plane, (c) microstrip line, and (d) side view of the antenna.

Table 1: The geometry data of the proposed antenna.

a (mm)	g	p (mm)	r_1 (mm)	r_2 (mm)	l_1 (mm)	w	α_1	α_2
50	0.5 mm	7.3	4.6	5.6	25	1.5 mm	45°	14°

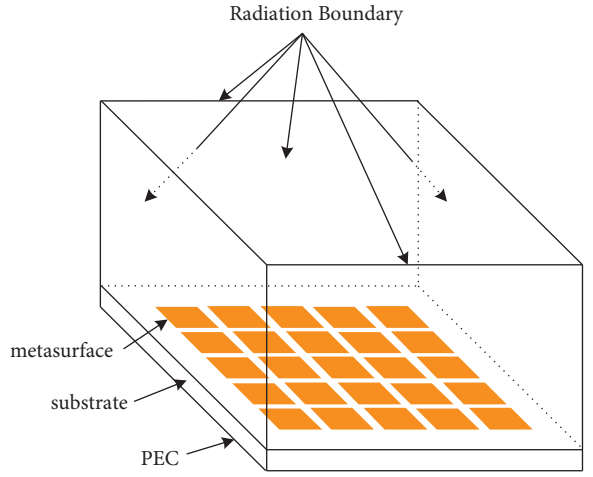

Figure 2: A simulation model of the metasurface and boundary setup.

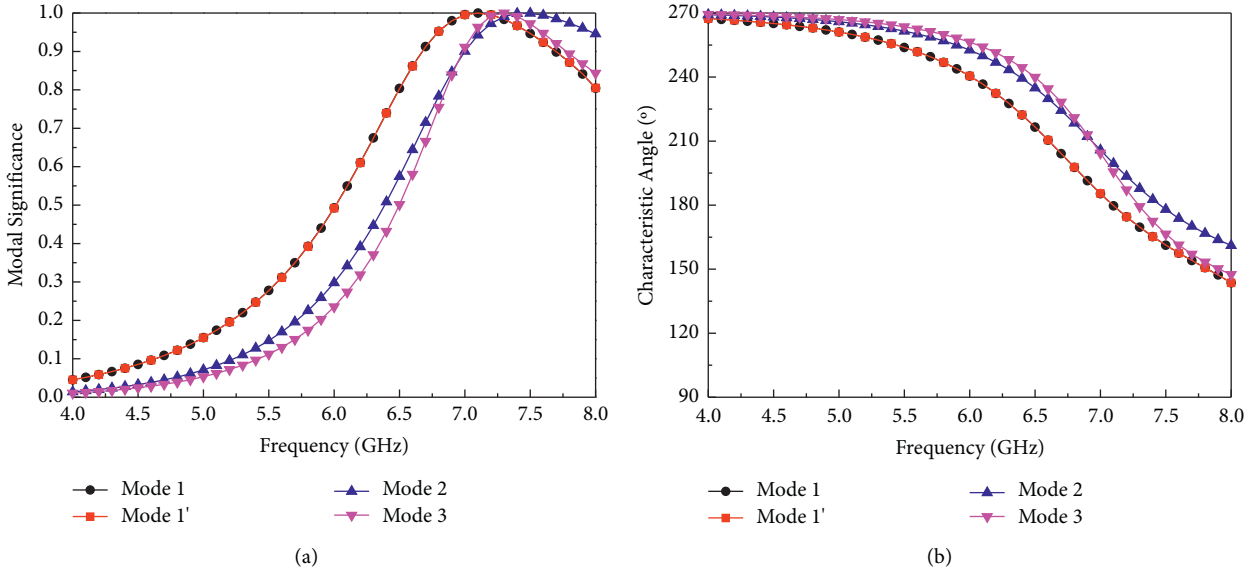

Figure 3: (a) The modal significance and (b) the characteristic angle of the proposed metasurface.

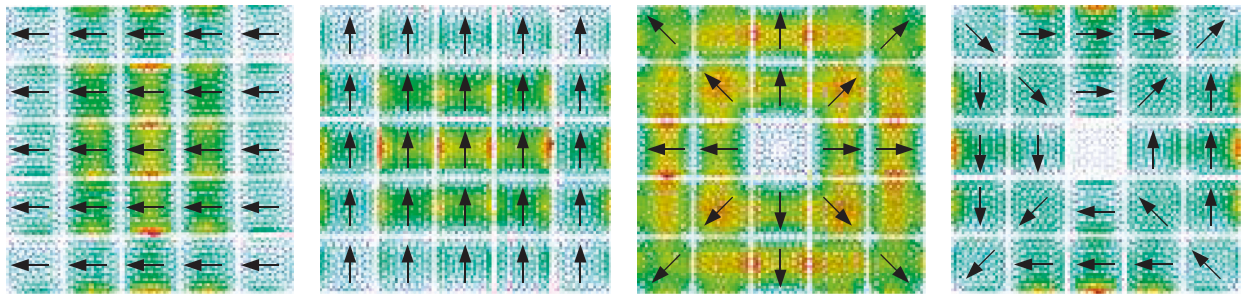

(a) (b) (c) (d)

Figure 4: Schematic representations of the modal currents of the developed metasurface at 6.8 GHz. (a) J_1 (b) J_1' (c) J_2 (d) J_3.

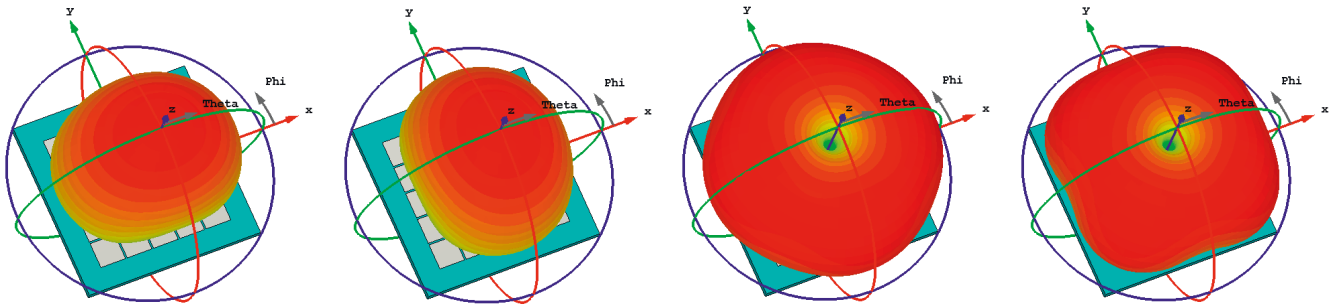

(a) (b) (c) (d)

Figure 5: The modal radiation patterns of the proposed metasurface at 6.8 GHz. (a) J_1 (b) J_1' (c) J_2 (d) J_3.

minimum points for each spacing g. The left one shift towards higher frequency as the spacing is increased, and the right one keeps at 6.8 GHz. An optimized value of the spacing must therefore be selected to obtain the desired AR bandwidth.

4. Results and Discussion

In order to verify the analysis above, one prototype is fabricated, as shown in Figure 8. The bottom and top views of the antenna are presented in the right and left images, respectively. The S-parameters are evaluated using an Agilent E5071C network analyzer. Figure 9 presents the measured and simulated S-parameters varying in terms of the frequency. The measured −10 dB S_{11} bandwidth is a little wider than the simulated results, which is 43.9% at the center frequency of 6.15 GHz (4.8–7.5 GHz). There are a few discrepancies between these two results but share a similar variation as a function of the frequency. Such divergence can be caused by the fabrication tolerance, including the adhesive glue and small distance between PCBs.

Figure 10(a) shows the comparison between the simulated and measured ARs and antenna gains. The obtained findings demonstrate that the developed antenna has an AR bandwidth of 22.2% (5.6–7.0 GHz), while the simulated coverage is in the range of 5.6 to 6.9 GHz (20.8%). The measurements show the ARs of 0.30 and 0.86 dB at 6.8 and 5.8 GHz, respectively. There is only a slight discrepancy between the measured and simulated ARs. The minimum AR point at 5.8 GHz is mainly caused by the shorted annular-ring slot antenna, and the higher one at 6.8 GHz is generated by the metasurface, resulting in broadband circularly polarized radiation. As shown in Figure 11, the measured boresight gains are more than 7.4 dBic within the CP radiation bandwidth, yielding the highest gain of 9.3 dBic at 6.9 GHz. The gain increment of the antenna with the increasing frequency (5.6–6.9 GHz) and high gain performance are attributed to the effective excitation of the orthogonal modes. As shown in Figure 10(b), the simulation and the measurement radiation efficiency are both higher than 87% throughout the 3-dB AR bandwidth.

The simulated and measured far-field radiation patterns of the antenna at 5.8 and 6.8 GHz have been plotted in Figure 11. The antenna produces stable and symmetrically unidirectional boresight radiation patterns with LH CP radiation. No obvious difference is observed between the simulated and measured radiation patterns. At both frequency points, the LH CP radiation is higher than the right-hand CP radiation. At the frequency of 5.8 GHz, the measurement yields a front-to-back ratio of 19.5 dB, a gain of 7.52 dBic, and a half-power beamwidth (HPBW) of 68° in both *xoz* and *yoz* planes. Furthermore, at the frequency of 6.8 GHz, the measurement yields a gain of 9.20 dBic, a front-to-back ratio of 35.8 dB, and a HPBW of 48° in both *xoz* and *yoz* planes.

Table 2 indicates the comparison between the results of the developed antenna and other CP metasurface antennas. Compared with [10, 12, 23], the developed antenna exhibits the highest gain. On the other hand, the developed antenna has a

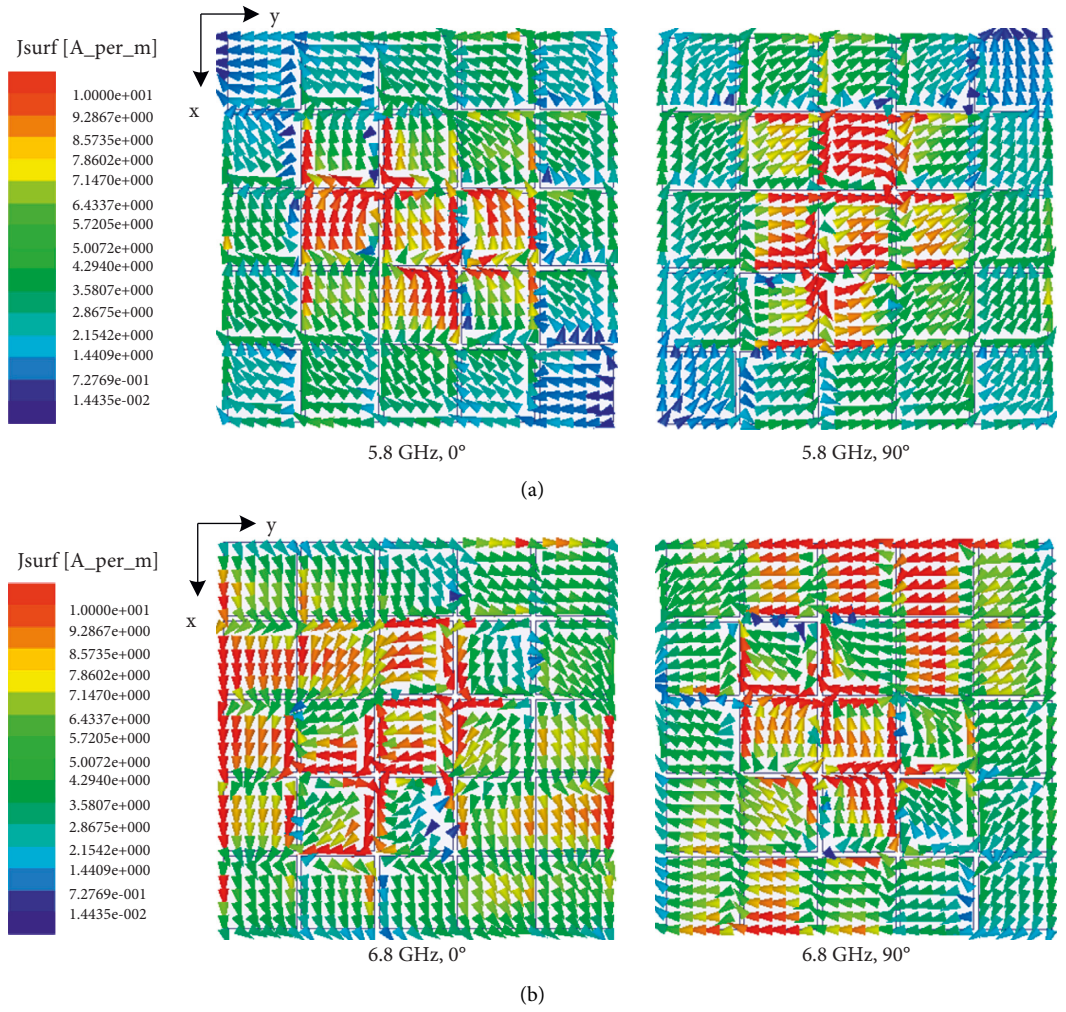

Figure 6: The current distributions on the metasurface for various phase angles: (a) 5.8 GHz and (b) 6.8 GHz.

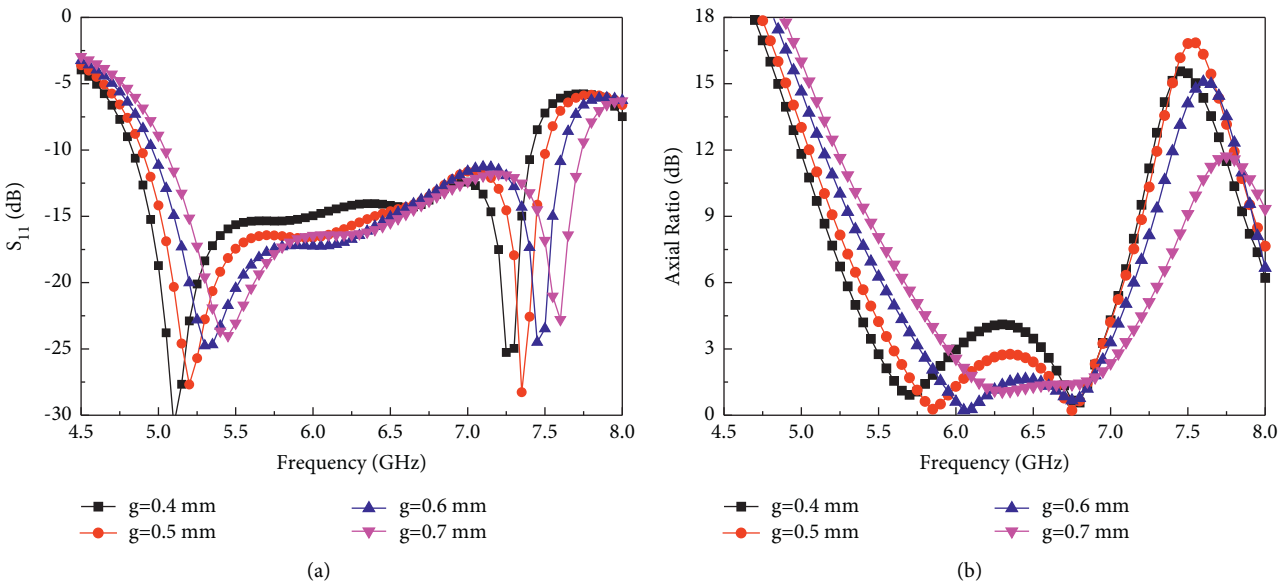

Figure 7: (a) S_{11} and (b) AR versus frequency for different spacing g.

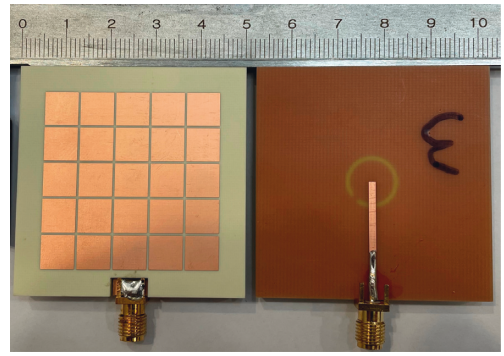

Figure 8: The photographs of the proposed antenna for various views; left: top view; right: bottom view.

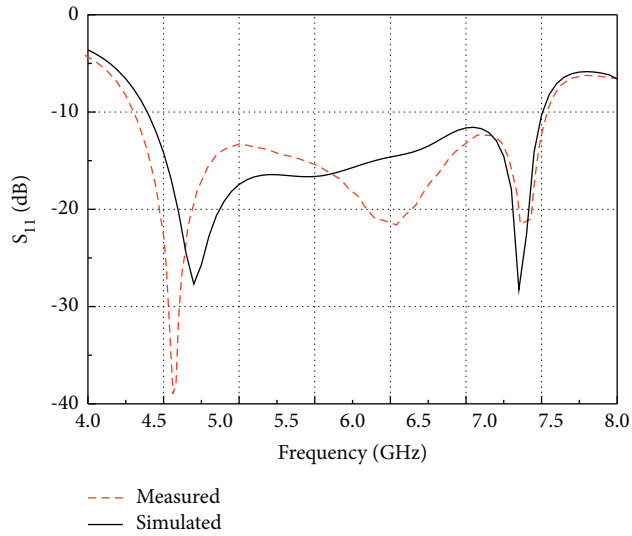

Figure 9: The measured/simulated reflection coefficients.

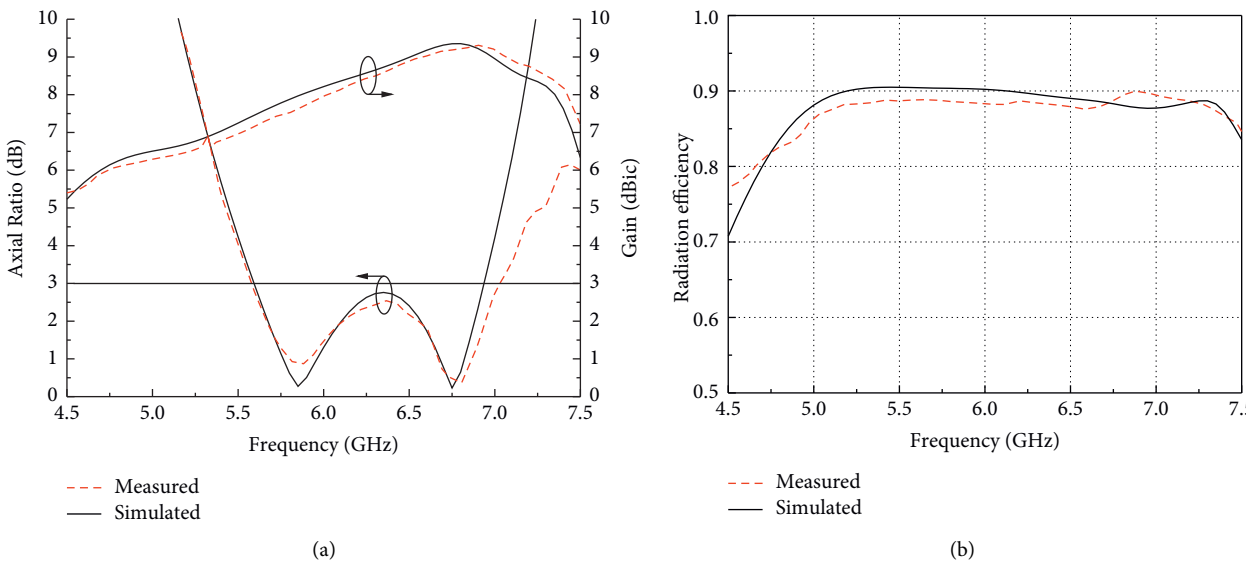

Figure 10: The measured/simulated (a) gain and ARs and (b) radiation efficiency.

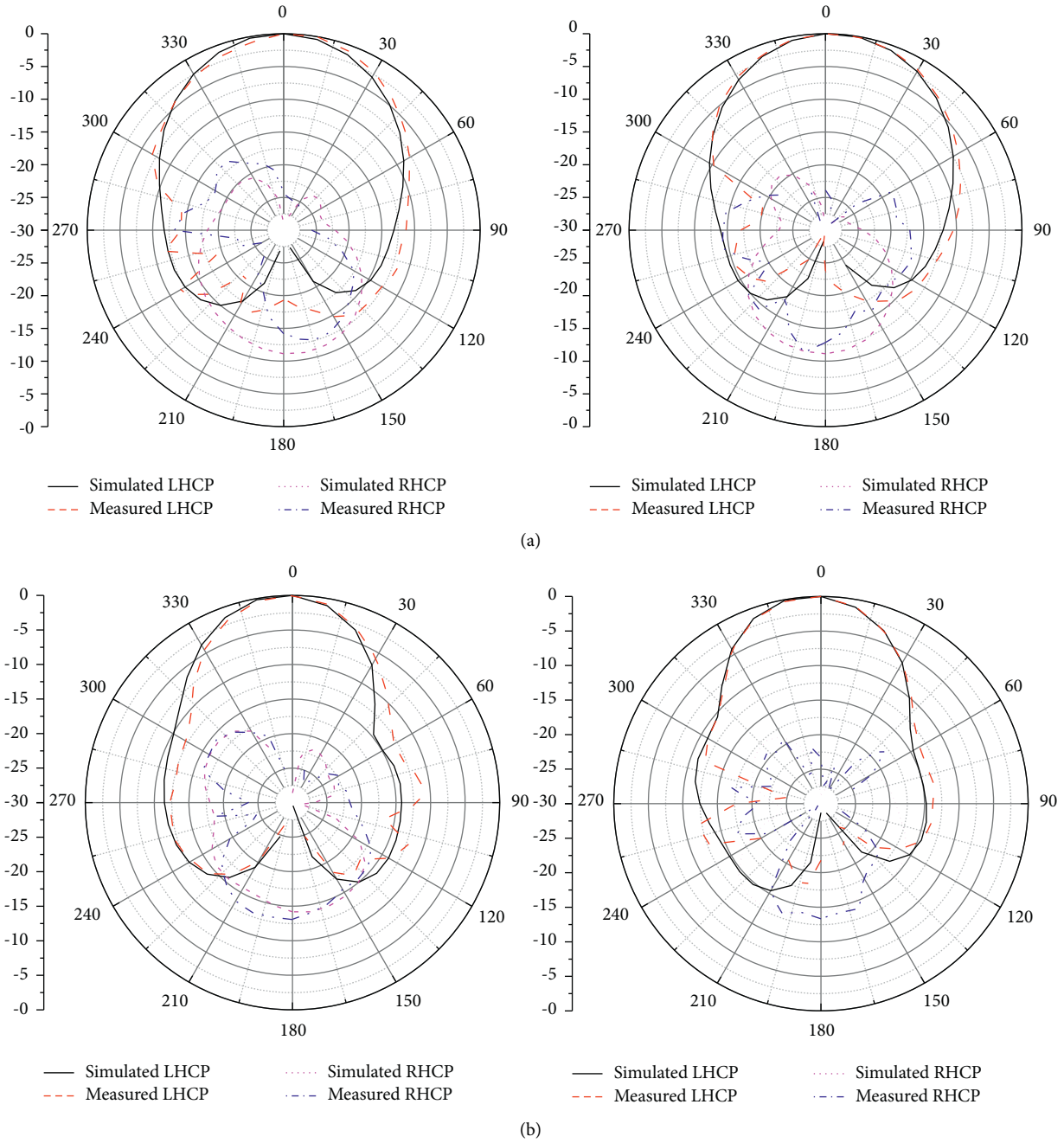

Figure 11: The measured and simulated radiation patterns of the antenna at: (a) 5.8 GHz and (b) 6.8 GHz.

Table 2: Comparison of the developed antenna with other studied antennas.

Ref	Size (λ^3)	Frequency (GHz)	Impedance Bandwidth (%)	3-dB ARBW (%)	Peak gain (dBic)
[10]	$0.58 \times 0.58 \times 0.056$	5.5	45.6	23.4	7.6
[11]	$1.4 \times 1.4 \times 0.071$	5.6	38.8	14.3	9.4
[12]	$0.93 \times 0.93 \times 0.024$	1.51	17	14.5	8.0
[13]	$1.0 \times 1.0 \times 0.07$	5.5	28.2	20.9	9.7
[20]	$1.1 \times 1.1 \times 0.093$	26.8	34.7	20.1	11
[21]	$1.0 \times 1.0 \times 0.04$	27.3	23.4	16.8	11
[22]	$0.86 \times 0.67 \times 0.13$	5.6	22.6	14.3	4.8
[23]	$0.94 \times 0.94 \times 0.06$	5.9	40.7	27.1	7.2
[24]	$0.822 \times 1.18 \times 0.06$	4.0	36	28.3	7.5
This work	$1.05 \times 1.05 \times 0.059$	6.3	43.9	22.2	9.3

broader 3-dB AR bandwidth but is still lower than that of the antenna studied in [10]. Generally, the designed antenna exhibits a satisfactory overall performance, including wide bandwidth, high gain, and LP.

5. Conclusions

A single-feed, high gain, LP, and broadband CP metasurface antenna was presented. The modal behavior of the metasurface (5×5 metal plates) was investigated by the CMA. In the meantime, a feeding structure contained a microstrip line, and a shorted annular-ring slot was utilized to excite the desired orthogonal modes. They produced a PD of 90° between them, leading to a circularly polarized radiation. For the sake of verification, a prototype antenna was also designed and tested. The prototype, $1.05\lambda_0 \times 1.05\lambda_0 \times 0.059\lambda_0$ at 6.3 GHz, attains an impedance bandwidth of 43.9% for $|S11| < -10$ dB, a broadside gain of 7.4–9.3 dBic, and a 3-dB AR bandwidth of 22.2%. The developed antenna exhibited unique properties of the LP, appropriate impedance similarity, broad CP-radiation bandwidths, and high gain.

Data Availability

The data used to support the findings of this study are included within the article.

Conflicts of Interest

The authors declare that they have no conflicts of interest.

Acknowledgments

This work was supported by the Science Research Project of Education Department of Anhui Province (No. KJ2021A1024) and the Domestic Visiting Study Program for Outstanding Young Talents in Colleges (No. gxgnfx2021145).

References

[1] N. Nasimuddin, X. Qing, and Z. N. Chen, "Dual-square-ring-shaped slot antenna for wideband circularly polarized radiation," *Microwave and Optical Technology Letters*, vol. 56, no. 11, pp. 2645–2649, 2014.

[2] S. Trinh-Van, Y. Yang, K. Y. Lee, and K. C. Hwang, "Broadband circularly polarized slot antenna loaded by a multiple-circular- sector patch," *Sensors*, vol. 18, no. 5, p. 1576, 2018.

[3] W. S. Chen, C. C. Huang, and K. L. Wong, "Microstrip-line-fed printed shorted ring-slot antennas for circular polarization," *Microwave and Optical Technology Letters*, vol. 31, no. 2, pp. 137–140, 2001.

[4] C. S. Lin, L. T. Chen, T. R. Chen, and J. S. Row, "Dual-band ring slot antenna with circular polarization," *Microwave and Optical Technology Letters*, vol. 55, no. 9, pp. 2077–2080, 2013.

[5] K. W. Leung, "Circularly polarized dielectric resonator antenna excited by a shorted annular slot with a backing cavity," *IEEE Transactions on Antennas and Propagation*, vol. 52, no. 10, pp. 2765–2769, 2004.

[6] K. W. Leung and K. K. So, "Frequency-tunable designs of the linearly and circularly polarized dielectric resonator antennas using a parasitic slot," *IEEE Transactions on Antennas and Propagation*, vol. 53, no. 1, pp. 572–578, 2005.

[7] S. X. Ta and I. Park, "Artificial magnetic conductor-based circularly polarized crossed-dipole antennas: 2. AMC structure without grounding pins," *Radio Science*, vol. 52, no. 5, pp. 642–652, 2017.

[8] J. Chatterjee, A. Mohan, and V. Dixit, "Broadband circularly polarized H-shaped patch antenna using reactive impedance surface," *IEEE Antennas and Wireless Propagation Letters*, vol. 17, no. 4, pp. 625–628, 2018.

[9] S. S. Jash, C. Goswami, and R. Ghatak, "A low profile broadband circularly polarized planar antenna with an embedded slot realized on a reactive impedance surface," *AEU - International Journal of Electronics and Communications*, vol. 108, pp. 62–72, 2019.

[10] S. X. Ta and I. Park, "Low-profile broadband circularly polarized patch antenna using metasurface," *IEEE Transactions on Antennas and Propagation*, vol. 63, no. 12, pp. 5929–5934, 2015.

[11] C. Zhao and C. F. Wang, "Characteristic mode design of wide band circularly polarized patch antenna consisting of H-shaped unit cells," *IEEE Access*, vol. 6, pp. 25292–25299, 2018.

[12] S. Liu, D. Yang, and J. Pan, "A low-profile circularly polarized metasurface antenna with wide axial-ratio beamwidth," *IEEE Antennas and Wireless Propagation Letters*, vol. 18, no. 7, pp. 1438–1442, 2019.

[13] X. Gao, G. W. Tian, Z. Y. Shou, and S. L. Li, "A low-profile broadband circularly polarized patch antenna based on characteristic mode analysis," *IEEE Antennas and Wireless Propagation Letters*, vol. 20, no. 2, pp. 214–218, 2021.

[14] A. Sharma, D. Gangwar, B. K. Kanaujia, and S. Dwari, "Gain enhancement and broadband RCS reduction of a circularly polarized aperture-coupled annular-slot antenna using metasurface," *Journal of Computational Electronics*, vol. 17, no. 3, pp. 1037–1046, 2018.

[15] K. E. Kedze, H. Wang, and I. Park, "A metasurface-based wide-bandwidth and high-gain circularly polarized patch antenna," *IEEE Transactions on Antennas and Propagation*, vol. 70, no. 1, pp. 732–737, 2022.

[16] Z. Song, J. Zhu, L. Yang, P. Min, and F. H. Lin, "Wideband metasurface absorber (metabsorber) using characteristic mode analysis," *Optics Express*, vol. 29, no. 22, pp. 35387–35399, 2021.

[17] F. H. Lin and Z. N. Chen, "Resonant metasurface antennas with resonant apertures: characteristic mode analysis and dual-polarized broadband low-profile design," *IEEE Transactions on Antennas and Propagation*, vol. 69, no. 6, pp. 3512–3516, 2021.

[18] B. B. Q. Elias, P. J. Soh, A. A. Al-Hadi, P. Akkaraekthalin, and G. A. E. Vandenbosch, "A review of antenna analysis using characteristic modes," *IEEE Access*, vol. 9, pp. 98833–98862, 2021.

[19] M. Cabedo-Fabres, E. Antonino-Daviu, A. Valero-Nogueira, and M. Bataller, "The theory of characteristic modes revisited: a contribution to the design of antennas for modern applications," *IEEE Antennas and Propagation Magazine*, vol. 49, no. 5, pp. 52–68, 2007.

[20] N. Hussain, M. J. Jeong, A. Abbas, T. J. Kim, and N. Kim, "A metasurface-based low-profile wideband circularly polarized patch antenna for 5G millimeter-wave systems," *IEEE Access*, vol. 8, pp. 22127–22135, 2020.

[21] N. Hussain, M. J. Jeong, A. Abbas, and N. Kim, "Metasurface-based single-layer wideband circularly polarized MIMO

antenna for 5G millimeter-wave systems," *IEEE Access*, vol. 8, pp. 130293–130304, 2020.

[22] N. Hussain, S. I. Naqvi, W. A. Awan, and T. T. Le, "A metasurface-based wideband bidirectional same-sense circularly polarized antenna," *International Journal of RF and Microwave Computer-Aided Engineering*, vol. 30, no. 8, Article ID e22262, 2020.

[23] H. Hung Tran, K. Nguyen-Dang, and N. Hussain, "Single-layer wideband circularly polarized antenna using non-uniform metasurface for c-band applications," *Computers, Materials & Continua*, vol. 68, no. 2, pp. 2487–2498, 2021.

[24] N. Nasimuddin, Z. N. Chen, and X. Qing, "Bandwidth enhancement of a single-feed circularly polarized antenna using a metasurface: metamaterial-based wideband CP rectangular microstrip antenna," *IEEE Antennas and Propagation Magazine*, vol. 58, no. 2, pp. 39–46, 2016.